Energy partition in low energy fission

M. Mirea
Horia Hulubei National Institute for Physics and Nuclear Engineering, RO-077125 Bucharest, Romania
(Received 15 February 2011; revised manuscript received 25 March 2011; published 18 May 2011)

The intrinsic excitation energy of fission fragments is dynamically evaluated in terms of the time-dependent pairing equations. These equations are corroborated with two conditions. One of them fixes the number of particles and the other separates the pairing active spaces associated to the two fragments in the vicinity of the scission configuration. The fission path is obtained in the frame of the macroscopic-microscopic model. The single-particle-level schemes are obtained within the two-center Woods-Saxon shell model. It is shown that the available intrinsic dissipated energy is not shared proportionally to the masses of the two fission fragments. If the heavy fragment possesses nucleon numbers close to the magic ones, the accumulated intrinsic excitation energy is lower than that of the light fragment.

DOI: 10.1103/PhysRevC.83.054608 PACS number(s): 24.75.+i, 21.60.Cs, 24.10.Cn, 24.10.Eq

I. INTRODUCTION

Under the action of a mutual Coulomb repulsion, at scission the fission fragments are accelerated in opposite directions. These fragments are highly excited, as underlined in many review papers, for example in Refs. [1,2]. The maximal kinetic energy issued in the process amounts to the Q value in the case of cold fission. The fragments decay on their ground states mainly by evaporation of neutrons and by radiation emission. It is known that the motion of any physical system is governed by conservative forces and by frictional ones that give rise to dissipation. Consequently, the excitation energy of the fragments must depend on the dynamics of the nuclear system in its path to scission.

The fission process offers a possibility to investigate how two nuclei in contact share their excitation energy. In analyses of experimental data, the authors of Ref. [3] evidenced an energy sorting mechanism based on statistical arguments. Considering a postulated difference between the temperatures of the two nascent fragments in conjunction with the condition of maximum entropy, they emphasized a flow of energy from one fragment to another. This flow of energy depends on the available states in the fragments in the scission configuration. In this context, an explanation for the violation of the constant-temperature hypothesis [4] that involves a proportionality between the intrinsic excitation energy division and the mass ratio of the fragment is offered.

Experimental direct indications about the excitation energies of the fragments are obtained by measuring their evaporated neutrons [5]. Despite a similar temperature of the neutron velocity distributions, the experiment revealed that a larger excitation energy characterizes the light mass distribution in comparison with the heavy one. The shifting in the sawtoothlike behavior of the neutron multiplicity as a function of the parent excitation was attributed mainly to the deformation energy and not to the intrinsic heat. The thermal neutron-induced fission of ^{233}U [6] analyzed in Ref. [7] evidenced a small neutron multiplicity in the $A = 132$ region. By increasing the excitation energy of the compound nucleus, it was observed that in this mass region the kinetic energy decreases by a large value of about 2 MeV. The interpretation ascribed a similar temperature of fragments as scission and it was speculated that this increment in excitation energy is due to a modification of the shape sequences during fission leading to a deformed heavy fragment. Furthermore, the multiplicity obtained for two neutron-induced ^{237}Np fission energies [8] revealed a modification of the heat of only the fragments in the heavier mass distribution.

Motivated by these aspects, in this work, the intrinsic excitation energy of the fragments are evaluated dynamically in terms of time-dependent pairing equations (TDPEs) in the cold fission regime. The macroscopic-microscopic model is employed to obtain the fission path by using the minimal action principle. The method is briefly described in the next section. The basic ingredients for the TDPE are the single-particle diagrams that must be computed from the initial state of the fissioning nucleus up the configuration given by two separated fragments. The Woods-Saxon two-center shell model [9] used to determine realistic level schemes along the fission path is presented in Sec. III. In Sec. IV, the formalism concerning the TDPE is introduced and its relevance in calculating dissipation energy is emphasized. In Sec. V, the formalism is extended for two separated nuclei. In Sec. VI, the results concerning the ^{234}U fission are reported. The last section is devoted to conclusions.

II. THE FISSION TRAJECTORY

To calculate the energy-level diagrams for the fissioning system, the first step is the determination of a fission path that satisfies the minimal action criteria [10]. The sequence of shapes that follows a nucleus when it passes from the ground state to the scission point depends principally on the potential energy surface and the inertia.

In the macroscopic-microscopic method, the whole system is characterized by some collective coordinates that determine approximately the behavior of many other intrinsic variables. The basic ingredient in such an analysis is a nuclear shape parametrization that depends on several macroscopic degrees of freedom. The generalized coordinates associated with these degrees of freedom vary in time, leading to a split of the nuclear system in two separated fragments.

In the following, an axially symmetric nuclear shape is obtained by smoothly joining two spheroids of semiaxis a_i and

b_i $(i = 1, 2)$ with a neck surface generated by the rotation of a circle around the axis of symmetry. By imposing the condition of volume conservation we are left with five independent generalized coordinates $\{q_i\}$ $(i = 1, 5)$ that can be associated to five degrees of freedom: the elongation R given by the distance between the centers of the spheroids, the necking parameter $C = S/R_3$ related to the curvature of the neck, the eccentricities ϵ_i associated with the deformations of the nascent fragments, and the mass asymmetry parameter $\eta = a_1/a_2$. The notations that describe this parametrization can be identified by inspecting Fig. 1. Owing to the axial symmetry, the surface equation is given in cylindrical coordinates for the three regions involved:

$$\rho(z) = \begin{cases} b_1\sqrt{1-(z-z_1)^2/a_1^2}, & z \leqslant z_{c1}, \\ \rho_3 - S\sqrt{R_3^2-(z-z_3)^2}, & z_{c1} < z < z_{c2}, \\ b_2\sqrt{1-(z-z_2)^2/a_2^2}, & z \geqslant z_{c2}. \end{cases} \quad (1)$$

It is known that a nuclear shape is well adapted for the fission process if the following conditions are satisfied [11]: (i) the three most important degrees of freedom, that is, elongation, necking, and mass asymmetry, are taken into account; (ii) a single sphere and two separated fragments are allowed configurations; and (iii) the flatness of the neck is an independent variable. All these conditions are fulfilled by the preceding parametrization. If $S = 1$, the shapes are necked in the median surface, characterizing scission shapes; for $S = -1$, the shapes are swollen, addressing the ground state and the saddle configurations.

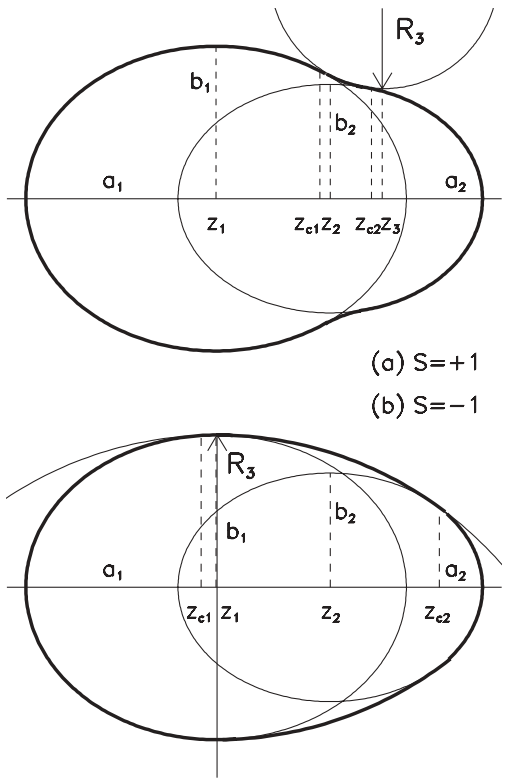

FIG. 1. Nuclear shape parametrization. Two ellipsoids of different eccentricities are smoothly joined with a third surface. Two cases are obtained: (a) the curvature of the neck is positive $(S = 1)$ and (b) the curvature is negative $(S = -1)$.

If we consider that the elongation $q_1 = R$ is the main coordinate, the dependencies of the other generalized coordinates $q_i = f_i(R)$ $(i = 2, 5)$ must be obtained. As specified in Ref. [10], such trajectories emerge by minimizing the action functional

$$P = -\frac{2}{\hbar}\int_{R_i}^{R_f}\sqrt{2M(q_i, \partial q_i/\partial R)V(q_i)}\,dR, \quad (2)$$

where $M(q_i, \partial q_i/\partial R)$ is the inertia along the trajectory and $V(q_i)$ is the deformation energy; R_i and R_f stand for the elongations associated to the ground state and to the exit from the barrier, respectively. In our calculation, the reference of the deformation energy is always taken as the energy in the ground state. So the next condition is fulfilled: $V(R_i) = V(R_f) = 0$. As it can be seen in Eq. (2), as the fissioning nucleus passes from its ground state to the scission configuration, the sequences of shapes depends mainly on the deformation energy and the inertia. The deformation energy is obtained in the frame of the macroscopic-microscopic model [12], whereas the inertia is computed within the cranking approximation [10,13,14]. The deformation energy was obtained by summing the liquid drop energy $E_{\rm LDM}$ with the shell and the pairing corrections δE:

$$V = E_{\rm LDM} + \delta E. \quad (3)$$

The macroscopic energy $E_{\rm LDM}$ is obtained in the framework of the Yukawa-plus-exponential model [15] extended for binary systems with different charge densities as detailed in Ref. [16]:

$$E_{\rm LDM} = E_n + E_C + E_V, \quad (4)$$

where

$$E_n = -\frac{a_2}{8\pi^2 r_0^2 a^4}\int_v\int_v\left(\frac{r_{12}}{a}-2\right)\frac{\exp\left(-\frac{r_{12}}{a}\right)}{\frac{r_{12}}{a}}d^3r_1 d^3r_2 \quad (5)$$

is the nuclear term,

$$E_C = \frac{1}{2}\int_v\int_v\frac{\rho_e(\vec{r}_1)\rho_e(\vec{r}_2)}{r_{12}}d^3r_1 d^3r_2 \quad (6)$$

is the Coulomb energy, and E_V is the volume energy. In the previous definitions, ρ_e are charge densities and $r_{12} = |\vec{r}_1 - \vec{r}_2|$. The numerical values of the parameters a_2, r_0, and a are taken from Ref. [17].

The shell effects δE are obtained as a sum between the shell and the pairing microscopic corrections. In this context, the Strutinsky procedure [10] was used. These corrections represent the varying parts of the total binding energy caused by the shell structure. The single-particle-level diagrams are computed within the Woods-Saxon superasymmetric two-center shell model.

The effective mass is computed within the cranking adiabatic approximation [10,13,14]. In a multidimensional deformation space, where the nuclear shape is described by the set of n independent generalized coordinates q_i, the inertia

tensor M_{ij} is defined by the equation of the kinetic energy T:

$$T = \frac{1}{2}\sum_{i,j=1}^{n} M_{ij}(q_1,\ldots,q_n)\frac{\partial q_i}{\partial t}\frac{\partial q_j}{\partial t}. \quad (7)$$

In the adiabatic description of the collective behavior of a nucleus, the nucleons are assumed to move in an average deformed potential. Using a Hamiltonian $H(q_1,\ldots,q_n)$ that includes pairing interactions, introducing the collective parameters q_i by means of the Lagrange multipliers, it is possible to obtain the response of the nuclear system for slow changes of the shape within the cranking model formula

$$M_{ij}(q_1,\ldots,q_n) = \frac{2}{\hbar^2}\sum_{\nu,\mu}\frac{\langle\mu|\frac{\partial H}{\partial q_i}|\nu\rangle\langle\nu|\frac{\partial H}{\partial q_j}|\mu\rangle}{(E_\mu+E_\nu)^3} \times (u_\mu v_\nu + u_\nu v_\mu)^2 + P_{ij}, \quad (8)$$

where $|\nu\rangle$ and $|\mu\rangle$ are single-particle wave functions; E_ν, u_ν, and v_ν are the quasiparticle energy, and the vacancy and occupation amplitudes of the state ν, respectively, in the BCS approximation; and P_{ij} is a correction that depends on the variation of the pairing gap and the Fermi energy as a function of the deformation coordinates. Recently, Eq. (8) was generalized by taking into account the intrinsic excitation produced during the fission process itself [18]. The inertia M along a trajectory in the configuration space spanned by the generalized coordinates q_i $(i = 1, 5)$ can be obtained within the formula

$$M = \sum_{i=1}^{5}\sum_{j=1}^{5} M_{ij}\frac{\partial q_i}{\partial R}\frac{\partial q_j}{\partial R}. \quad (9)$$

The total inertia is the sum of the contributions that correspond to the proton and to the neutron level schemes. Usually, the matrix elements of the derivatives of the Hamiltonian in Eq. (8) are replaced by the matrix elements of the derivatives of the mean field potential alone.

III. SINGLE-PARTICLE ENERGIES

A microscopic potential must be constructed to be consistent within our nuclear shape parametrization. The simplest way is to use a semiphenomenological Woods-Saxon potential. To take into account nuclear deformations going over to separate shapes and to obtain two separated fragments, a two-center shell model with a Woods-Saxon potential was developed recently [9]. Other recipes that allow treatment of strongly deformed nuclei are presented in Refs. [19,20]. The mean field potential is defined in the frame of the Woods-Saxon model:

$$V_0(\rho,z) = -\frac{V_c}{1+\exp\left[\frac{\Delta(\rho,z)}{a}\right]}, \quad (10)$$

where $\Delta(\rho,z)$ represents the distance between a point (ρ,z) and the nuclear surface. This distance is measured only along the normal direction on the surface and it is negative if the point (ρ,z) is located in the interior of the nucleus. The variable V_c is the depth of the potential while a is the diffuseness parameter. In our work, the depth is $V_c = V_{0c}[1 \pm \kappa(N_0 - Z_0)/N_0 + Z_0)]$, where the plus sign is for protons and the minus sign is for neutrons; $V_{0c} = 51$ MeV, $a = 0.67$ fm, and $\kappa = 0.67$. Here A_0, N_0, and Z_0 represent the mass number, the neutron number, and the charge number of the parent, respectively. This parametrization, referred as the Blomqvist-Walhlborn parametrization in Ref. [21], is adopted because it provides the same radius constant r_0 for the mean field and the pairing field, which ensures a consistency of the shapes of the two fields at hyperdeformations, i.e., two tangent ellipsoids. The Hamiltonian is obtained by adding the spin-orbit and the Coulomb terms to the Woods-Saxon potential. The eigenvalues are obtained by diagonalization of the Hamiltonian in the semisymmetric harmonic two-center basis [22–24]. In this work, the major quantum number used is $N_{\max} = 12$. The two-center Woods-Saxon model is used to compute shell and pairing corrections together with inertia in this work. The two-center shell model represents a valuable instrument to investigate the role of individual orbitals in the treatment of a wide variety of nuclear processes like cold fission [25], the formation of superheavy elements [26], or superasymmetric disintegration processes, pertaining to cluster and α decays [27–29].

IV. TIME-DEPENDENT PAIRING EQUATIONS

In the following formalism, the starting point is a many-body Hamiltonian with pairing residual interactions. This Hamiltonian depends on some time-dependent collective parameters $q(t) = \{q_i(t)\}$ $(i = 1,\ldots,n)$, such as the internuclear distances nuclei:

$$H(t) = \sum_{k>0}\epsilon_k[q(t)](a_k^+ a_k + a_{\bar{k}}^+ a_{\bar{k}}) - G\sum_{k,i>0} a_k^+ a_{\bar{k}}^+ a_i a_{\bar{i}}. \quad (11)$$

Here, ϵ_k are single-particle energies of the molecular potential, and a_k^+ and a_k denote operators for creating and destroying a particle in the state k, respectively. The state characterized by a bar signifies the time-reversed partner of a pair. The pairing correlation arises from the short-range interaction between fermions moving in time-reversed orbits. The essential feature of the pairing correction can be described in terms of a constant pairing interaction G acting between a given number of particles. In this article, the sum over pairs generally runs over the index k. Because the pairing equations diverge for an infinite number of levels, a limited number of levels is used in the calculation, that is, N levels above and below the Fermi energy E_F. In the following, $N = 30$.

To obtain the equations of motion, we start from the variational principle taking the following energy functional

$$\mathcal{L} = \langle\varphi|H - i\hbar\frac{\partial}{\partial t}|\varphi\rangle \quad (12)$$

by assuming the many-body state as a time-dependent BCS seniority-zero wave function

$$|\varphi(t)\rangle = \prod_k [u_k(t) + v_k(t)a_k^+ a_{\bar{k}}^+]. \quad (13)$$

To minimize this functional, expression (12) is derived with respect to the independent variables v_k, together with their complex conjugates, and the resulting equations are set to

zero. Eventually, the following TDPEs are obtained:

$$i\hbar\dot{\rho}_k = \kappa_k\Delta^* - \kappa_k^*\Delta,$$
$$i\hbar\dot{\kappa}_k = (2\rho_k - 1)\Delta - 2\kappa_k\epsilon_k, \tag{14}$$

where $\rho_k = |v_k|^2$ are occupation probabilities, $\kappa_k = u_k^* v_k$ are pairing moment components, and $\Delta = G\sum_k \kappa_k$ is the pairing gap; u_k and v_k are the complex BCS occupation and vacancy amplitudes. The variations of single-particle densities ρ_k can be evaluated for different values of the generalized velocities by solving the previous system of coupled equations as was done in Ref [30]. Equations (14) are also generically known as the time-dependent Hartree-Fock-Bogoliubov equations [31,32]. As mentioned in Ref. [32], a connection with the Landau-Zener effect is included in these equations. Levels undergo Landau-Zener transitions on virtual levels with coupling strengths given by the magnitude of the gap, Δ. Recently, these equations were generalized to take into account the Landau-Zener effect in seniority-one systems [9,33] and the pair-breaking mechanism [34].

These TDPEs can offer a measure of the average dissipated energy. The difference between the total energy value E obtained within the TDPE and E_0 given by the static BCS equations represents an approximate measure for the dissipation E^*:

$$E^* = E - E_0. \tag{15}$$

The total emergy E is expressed simply in terms of ρ_k and κ_k,

$$E = 2\sum_k \epsilon_k\rho_k - G\left|\sum_k \kappa_k\right|^2 - G\sum_k \rho_k^2; \tag{16}$$

E_0 corresponds to ρ_k^0 and κ_k^0 associated to the lower energy state, that is, obtained from BCS equations. This definition was introduced in Ref. [31], where the nuclear viscosity coefficient was determined by comparing microscopic results with hydrodynamic ones. In Ref. [30], a comparison between results given by Eq. (15) and experimental excitation energies of several fission fragments was made for the ^{236}U parent. For closed shell regions of fission fragments a very good agreement was found, the dissipated energies being 12–15 MeV. For symmetric fission, as expected, the calculated dissipation is greater than 20 MeV. Such agreement gives strong support for this model.

The sum of time derivatives of single-particle densities in Eqs. (14) is

$$i\hbar\sum_k \dot{\rho}_k = \sum_k [\kappa_k\Delta^* - \kappa_k^*\Delta]$$
$$= \frac{1}{G}[|\Delta|^2 - |\Delta|^2] = 0. \tag{17}$$

This result shows that the sum of the single-particle occupation probabilities is a constant quantity as the system evolves in time according to Eqs. (14); that is, the average number of particles in the pairing active level space is a constant of the motion.

V. NUMBER OF PARTICLES

After scission, the levels from the pairing active space are shared between the two fission fragments. The levels of the core are sorted accordingly. The sum of occupation probabilities of the levels located in each fragment must be equal to the number of nucleons. This is a problem that can be solved by appealing to two properties of the nuclear system.

First of all, the sorting is produced in a continuous manner: the wave function associated to one single-particle energy level is transferred gradually to one of the two potential wells obtained asymptotically, after the scission. For example, the Woods-Saxon wave function of the lowest single-particle energy is displayed in Fig. 2 for different values of the distance between the centers of the fragments, that is, for different shapes of the potential. When the two fragments are completely separated, the wave function is located in one of the two wells. Making use of this property, it is possible to identify the final localization of the single-particle level even when the system behaves as a single nucleus if the final mass asymmetry is known. For this purpose, we calculate two quantities $Q_{1k} = \langle\varphi_k(z)|\Theta(-z)|\varphi_k(z)\rangle$ and $Q_{2k} = \langle\varphi_k(z)|\Theta(z)|\varphi_k(z)\rangle$, where Θ is the Heaviside function

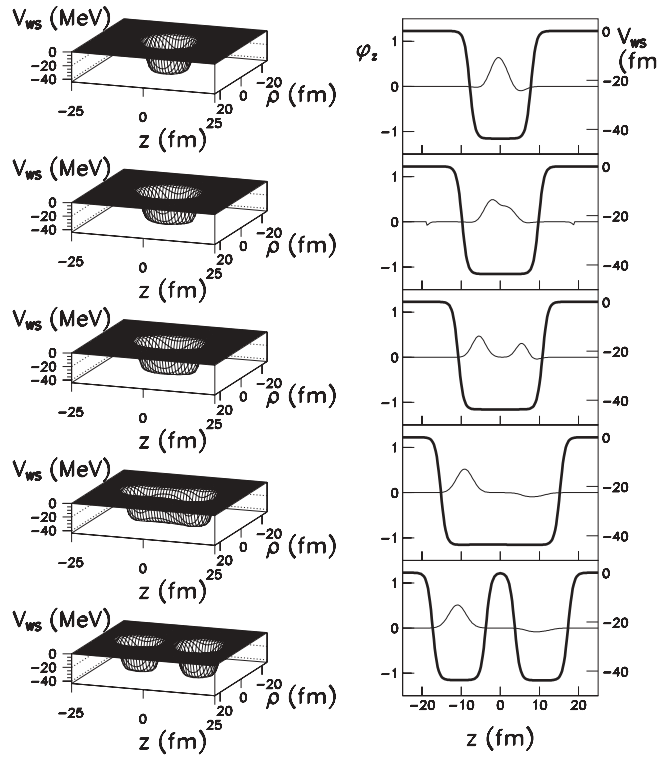

FIG. 2. (right) For the left axis, the lowest-energy Woods-Saxon wave function for the two center model $\varphi_0(z)$ as a function of z for different values of the distance between the centers is displayed with a thin line. The right axis corresponds to a plot with a thick curve of a section in the middle of the neutron Woods-Saxon potential $V_0(z)$ at the same values of the distance between centers. (left) A representation of the Woods-Saxon potential V_0 in the cylindrical ρ and z coordinates is made. The distances between centers R are 0, 6, 12, 18, and 21 fm from top to bottom. The configurations displayed correspond to the minimal ^{234}U fission trajectory.

and φ_k is the Woods-Saxon single-particle wave function of the state k along the axis z. If $Q_{1k} > Q_{2k}$, the wave function is located in well 1. It is worth noting that this procedure fails only in the avoided level-crossing regions.

Second, the matrix element of the pairing interaction G is in principle dependent on the overlap of the wave functions of the pairs [35,36]. In the simplest description, as long as a single nucleus is involved, the monopole approximation is considered to perform well [37] and all the values of the matrix elements are considered to have the same value in the active pairing space. However, after the scission, the matrix elements of the pairing interaction between wave functions belonging to states in different fragments must be zero. In general, the pairing interaction matrix elements of two different fragments are not the same. If the pairing matrix elements between pairs located in different fragments are zero ($G_{12} = 0$), then the energy given by Eq. (16) becomes

$$\begin{aligned} E &= 2\sum_k \epsilon_k \rho_k - G\left|\sum_k \kappa_k\right|^2 - G\sum_k \rho_k^2 \\ &\to 2\sum_{k_1} \epsilon_{k_1} \rho_{k_1} - G_1\left|\sum_{k_1} \kappa_{k_1}\right|^2 - G_1\sum_{k_1} \rho_{k_1}^2 \\ &\quad + 2\sum_{k_2} \epsilon_{k_2} \rho_{k_2} - G_2\left|\sum_{k_2} \kappa_{k_2}\right|^2 - G_2\sum_{k_2} \rho_{k_2}^2 \\ &= E_1 + E_2, \end{aligned} \tag{18}$$

where the sum over k_1 and k_2 means that the levels belong to fragments 1 and 2, respectively. We used an arrow in the previous relation to indicate that the constant value G of the parent nucleus can be also transformed in the two values G_1 and G_2 associated to the two fragments. In other words, the monopole approximation is considered valid separately in each fragment by considering two constant values of G_1 and G_2. Relation (18) shows that the total energy E is decomposed in two fragment total energies, E_1 and E_2, given by relations of the type of Eq. (16) if the value of the matrix element of the pairing interaction addressing different fragments is $G_{12} = 0$.

Within these properties, a simple recipe to fix the average number of particles at scission can be elaborated. Taking as an example the proton level scheme, the conditions that the sum of occupation probabilities of single-particle levels in the two wells must be equal to the number of nucleons of the fragments can be written as

$$\begin{aligned} 2Z_{p_2}\sum_{k_1} \rho_{k_1} &= 2Z_{p_1}\sum_{k_2} \rho_{k_2}, \\ Z_{p_1} + Z_{c_1} &= Z_1, \\ Z_{p_2} + Z_{c_2} &= Z_2, \end{aligned} \tag{19}$$

where Z_i $(i = 1, 2)$ are the numbers of protons in the two fragments, and Z_{c_i} and Z_{p_i} stand for the number of protons in the core and the number of protons in the pairing active space, respectively. For an initial number of protons $2N = Z_1 + Z_2$ considered in the pairing active space, the values of Z_{c_i} and Z_{p_1} are simply obtained by counting the levels given by the two-center shell model. The occupation probabilities ρ_{k_i} must be obtained from TDPE (14). Exploiting the two previous properties, the problem of fixing the final average number of particle within Eqs. (14) is now trivial. After the passage of the external saddle point, in the descent to scission, we insert condition (19) in functional (12) and we continue to solve the equations of motion. When the good numbers of particles are obtained, we impose the condition that G_{12} is zero between the wave functions belonging to separated fragments.

The previous recipe is implemented in the equations of motion in a very simple way. In the operator notation, condition (19) becomes

$$\begin{aligned} Z_{p_2}\hat{Z}_{p_1} &= Z_{p_1}\hat{Z}_{p_2}, \\ \hat{Z}_{p_1} &= \sum_{k_1}\left(a_{k_1}a_{k_1}^+ + a_{\bar{k}_1}a_{\bar{k}_1}^+\right), \\ \hat{Z}_{p_2} &= \sum_{k_2}\left(a_{k_2}a_{k_2}^+ + a_{\bar{k}_2}a_{\bar{k}_2}^+\right). \end{aligned} \tag{20}$$

This condition is introduced in the energy functional (12)

$$\mathcal{L} = \langle\varphi|H - i\hbar\frac{\partial}{\partial t} - \lambda\left(Z_{p_2}\hat{Z}_{p_1} - Z_{p_1}\hat{Z}_{p_2}\right)|\varphi\rangle \tag{21}$$

using a Lagrange multiplier λ. Imposing also the condition that the interaction matrix element $G_{12} \neq G_1 \neq G_2$, the new time-dependent equations eventually read

$$\begin{aligned} i\hbar\dot{\rho}_{k_1} &= \kappa_{k_1}\Delta_1^* - \kappa_{k_1}^*\Delta_1, \\ i\hbar\dot{\rho}_{k_2} &= \kappa_{k_2}\Delta_2^* - \kappa_{k_2}^*\Delta_2, \\ i\hbar\dot{\kappa}_{k_1} &= \left(2\rho_{k_1} - 1\right)\Delta_1 - 2\kappa_{k_1}\left(\epsilon_{k_1} - \lambda Z_{p_2}\right), \\ i\hbar\dot{\kappa}_{k_2} &= \left(2\rho_{k_2} - 1\right)\Delta_2 - 2\kappa_{k_2}\left(\epsilon_{k_2} + \lambda Z_{p_1}\right), \end{aligned} \tag{22}$$

where $\Delta_1 = G_1\sum_{k_1}\kappa_{k_1} + G_{12}\sum_{k_2}\kappa_{k_2}$ and $\Delta_2 = G_{12}\sum_{k_1}\kappa_{k_1} + G_2\sum_{k_2}\kappa_{k_2}$. When $G_{12} = 0$, it can be easily verified that Eq. (19) is fulfilled and that the average number of particles in the two fragments is conserved according to conditions of the type of Eqs. (17) applied separately on the two working spaces. That means, once the values Z_1 and Z_2 of a given partition are reached, they behave as constants if $G_{12} = 0$. The previous recipe represents the simplest dynamical method to project the average number of particles onto two separate nuclei. These equations are named time-dependent pairing equations with constraint (TDPEC).

VI. RESULTS

To obtain the fission trajectory, action integral (2) must be minimized in our five-dimensional space. The first turning point, R_i, is obtained by determining the ground-state configuration, while the second one, R_f, lies on the equipotential surface that characterizes the exit from the outer barrier. That means R_f is defined by the multidimensional function $V(R, C, \epsilon_1, \epsilon_2, \eta) = 0$. Different methods are currently envisaged to obtain the heights of the barriers. In static calculations [38], the immersion procedure is extensively used, whereas for dynamical paths [39–41], the Ritz method is applicable. To minimize the action integral, we used a numerical method initiated in Ref. [42] and used it for fission processes in a large range of mass asymmetries [34,43–45]. The dependencies

$C(R)$, $\epsilon_1(R)$, $\epsilon_2(R)$, and $\eta(R)$ were considered as spline functions of n variables C_k, ϵ_{1k}, ϵ_{2k}, and η_k ($k = 1, n$) that are associated to the fixed mesh points R_k located in the interval (R_i, R_j). The integral action is transformed in a numerical function that depends on the $4n$ variables and it is minimized numerically.

Determination of potential energies V and of effective masses M_{ij} are very expensive in computing time. For the numerical minimization procedure, a large number of iterations is required and it is not possible to calculate the values of V and M_{ij} for each iteration. An interpolation of calculated values of the energy and of the effective masses is used. Therefore, to make the problem tractable, first of all, a grid of deformation values was fixed in the five-dimensional configuration space: 25 values of R between 0 and 24 fm, 7 values of the eccentricities ϵ_i between 0 and 0.6, 7 values of the ratio η in the interval 1 to 1.6, and 23 values of C between -0.115 and 0.105 fm^{-1}. The pertinent region of deformations for the possible trajectories between the ground state and the exit point from the fission barrier was spanned. In each point of the configuration space, the deformation energy and the tensor of inertia were computed. During the minimization process, interpolated values of the deformation energy and the inertia were used. Different initial values of the generalized coordinates were used as input parameters for the minimization. Therefore, different local minima were obtained. The best value was selected. Moreover, additional calculations of the action integral were performed by slowing varying the generalized coordinates around the best trajectory previously obtained from the numerical procedure. Among all results, the best final trajectory for the least action was retained. Such a procedure was used in determining a theoretical system of fission barrier heights in Ref. [46]. In the present work, the trajectory in the configuration space was modified after the saddle of the outer barrier. The generalized coordinates were changed to obtain at scission a required final configuration, as explained later.

The minimization leads to a definite path in the subbarrier region. Its extrapolation to the scission point is not unique [47]. We choose two fission partners at scission by searching the best candidates that have deformations close to those obtained in the exit point of the barrier from minimization. We found that the eccentricities and mass-asymmetry parameters in the exit point of the outer barrier are consistent with the formation of a pair given by the isotopes ^{102}Zr and ^{132}Te. The ground-state configurations of the fragments were calculated for this purpose. It is known that the excitation energy has mainly two components: an excitation due to the deformations and an intrinsic one. So, by taking into account the ground-state deformations of the fragments at scission, the excitation due to the deformation energy is eliminated and we are only left with the dissipation. Comparing our theoretical result with an evaluation [48], we found that the partition $^{102}\mathrm{Zr} + {}^{132}\mathrm{Te}$ has a very probable yield. Moreover, this final configuration is also interesting because the numbers of nucleons in the heavy fragment are close to the magic ones. This configuration also allows a simple comparison with the hypothesis made in Ref. [3] concerning the excitation accumulated in a magic fission product. The fission barrier, together with some particular shapes, is plotted in Fig. 3.

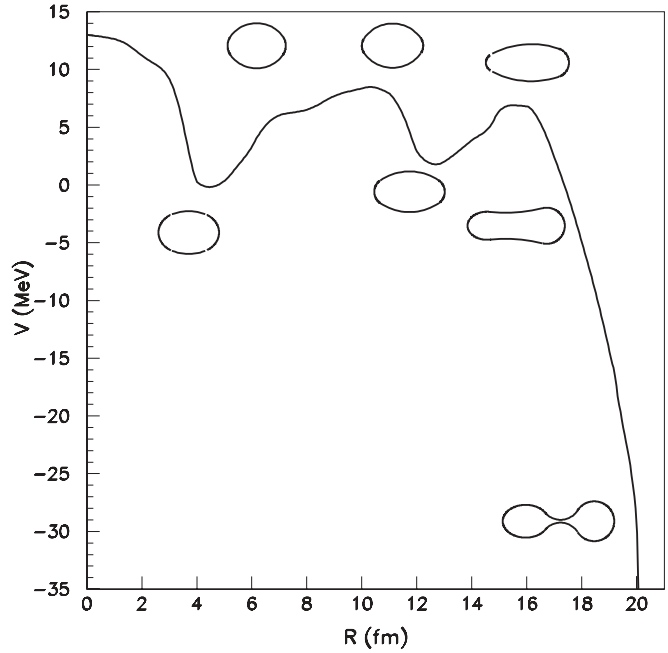

FIG. 3. ^{234}U fission barrier V for a final partition $^{102}\mathrm{Zr} + {}^{132}\mathrm{Te}$ determined along the minimal action trajectory. Some particular shapes related to the ground state, the extremes of the barrier, the exit point, and the scission point are inserted in the plot. The distances for the elongation R that characterizes the shapes are 4.17, 7.7, 10.43, 12.64, 15.53, 17.53, and 20.2 fm.

The neutron and proton single-particle diagrams are calculated along the minimal action trajectory, from the ground state of the parent up to the formation of two separated fragments. These level schemes are plotted in Figs. 4 and 5. In Fig. 4, at $R = 0$, the parent nucleus is considered spherical. For small deformations, the system evolves in a way similar to a Nilsson diagram for prolate deformations. In the left part of Fig. 4, the orbitals of the parent are labeled with their spectroscopic notations. The levels belonging to the heavy fragment can be identified before that the scission is produced, allowing us to plot them with thick lines. The heavy fragment is spherical at scission, so its levels are bounced in shells. Making use of the fact that the heavy fragment becomes spherical after scission, it is possible to label its orbitals with spectroscopic notations. The levels of the light fragment are not degenerate due to its deformation. In the proton diagram of Fig. 5, a smooth decrease of the single-particle energies after the scission due to the Coulomb mutual polarization can be observed. The energy slope for the light fragment is larger than that for the heavy one.

It is known that the projection on a given particle number changes the pairing coupling constant G [49]. For our exploratory investigation, constant values of the pairing matrix elements are kept for the parent nucleus and for the fragments without considering the variations due to projections. A renormalization procedure [10] in the BCS theory that depends on the energy level distribution and a smoothed gap distribution is used to obtain the values of G, G_1, and G_2 used in TDPEC (22).

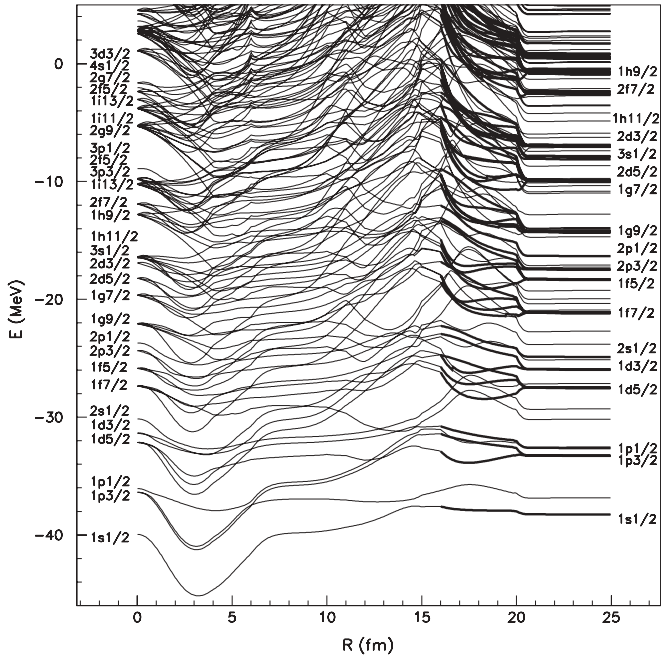

FIG. 4. Neutron level diagram for the ^{234}U fission with respect to the elongation R.

To solve TDPE (14), we need the velocity of the generalized coordinate. Our calculations pertain to the cold fission regime and are characterized by small values of the collective kinetic energy and of the excitations energies. These properties can be obtained by selecting an appropriate value for the collective velocity. Therefore, different constant values of the internuclear velocity $\dot{R}$ ranging from 10^4 to 10^6 m/s were tested. These values can be translated over a time to penetrate the barrier ranging in the interval $[10^{-18}, 10^{-20}]$ s. The time for the descent between saddle to scission reaches about 4×10^{-21} s for a velocity of 10^6 m/s, a value considered a typical time for scission [2]. Within the semiadiabatic cranking model [18], the inertias in the ground state and in the asymptotic region of two separated fragments are 1.26 and 1.208 $\hbar^2$ MeV^{-2} fm^{-2}, respectively. Within this estimation of the mass, the velocities can also be translated in a macroscopic kinetic energy that amounts to 0.3 MeV, of the order of magnitude of the zero point vibration energy. System (14) is solved numerically for the selected velocities. The initial conditions for ρ_k and κ_k are set by the ground-state BCS solutions of the parent, i.e., the configuration located at $R \approx 4$ fm in Fig. 3. In Fig. 6, the variations of the dissipated energy E^* for different internuclear velocities are displayed as a function of the distance between the centers of fragments, R. The TDPEs are solved and no conditions for fixing the number of particles are imposed here. The dissipated energy for the proton level scheme is lower than that of the neutron one. The dissipated energy for the lower collective velocity of 10^4 m/s is negligible, whereas for the largest one of 10^6 m/s the total dissipation reaches about 10.5 MeV at scission. This value is larger than that given in previous estimations [18] because of the imposed modification concerning the fission trajectory that gives a particular configuration at scission. In connection with the shape of the barrier displayed in Fig. 3, it can be deduced that the larger part of the excitation is formed during the penetration of the second barrier and in the descent from saddle to fission. This result is not in line with the hypothesis that the

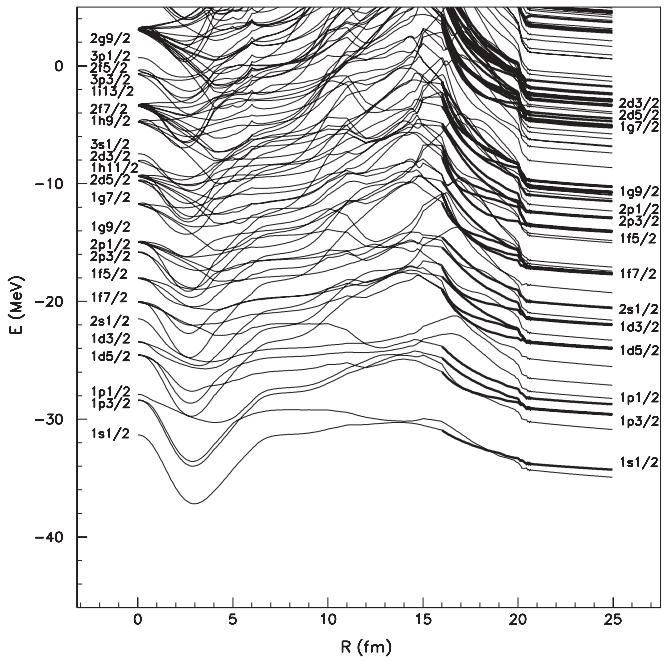

FIG. 5. Same as Fig. 4 for the proton diagram.

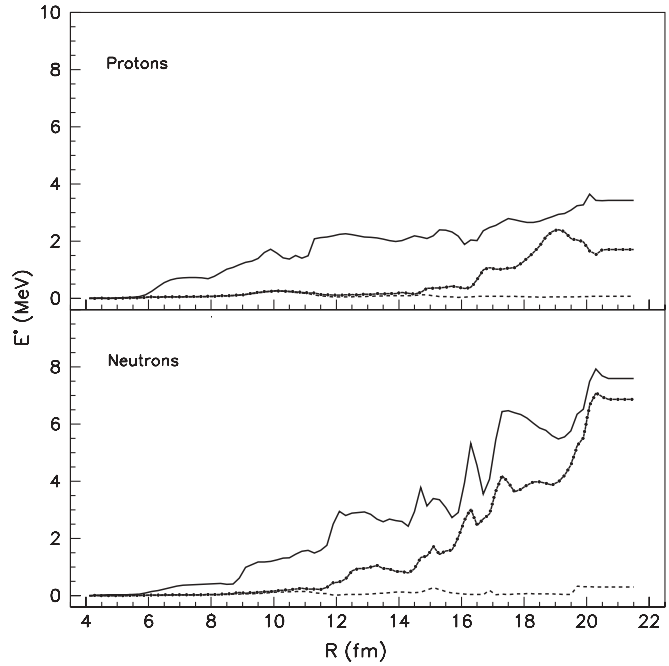

FIG. 6. Dissipation energy E^* calculated for the proton level scheme (top) and for the neutron one (bottom) as a function of the elongation R. The calculations are made within relation (15) and Eqs. (14) without imposing any condition for fixing the number of of particles. The dashed line, the dot-dashed line, and the solid line correspond to internuclear velocities dR/dt of 10^4, 10^5, and 10^6 m/s, respectively.

excitation energy does not increase after the passage of the saddle point [50]. Also, Fig. 6 evidences a strong correlation between the collective kinetic energy and the final excitation of the fragments: an increase in the kinetic energy produces an increase of the dissipation.

It is interesting to compare the dissipated energy and the number of nucleons attributed to the two nuclei in the case of the treatment with TDPE and that with TDPEC. In Fig. 7(a), the TDPE dissipation energy for the neutron workspace is plotted with a thick curve as a function of R at $dR/dt = 10^6$ m/s. The dissipation obtained within the TDPEC is displayed with a thin line. So, up to the external saddle, Eqs. (14) are solved. After $R \approx 16$ fm, we imposed condition (20), and the TDPEC was used. It can be observed that the TDPEC give a larger dissipation. In Fig. 7(b), the sums $N_{p_1} = \sum_{k_1} \rho^2_{k_1}$ and $N_{p_2} = \sum_{k_2} \rho^2_{k_2}$ for TDPEs are plotted with a thick line. As mentioned

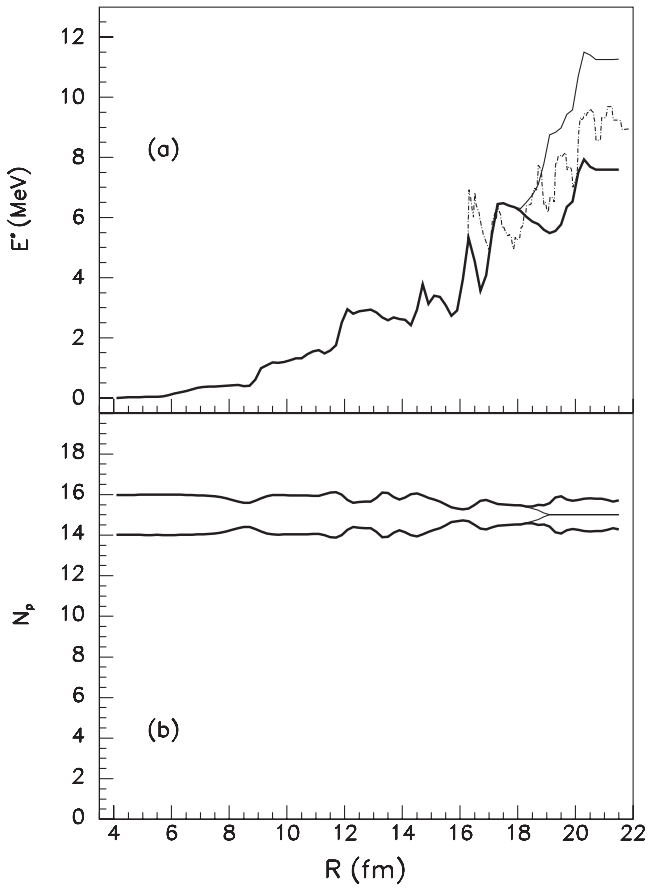

FIG. 7. (a) The TDPE dissipated energy is plotted with a solid thick line as a function of the elongation R for the neutron working space for the collective velocity $dR/dt = 10^6$ m/s. The TDPEC dissipated energy (after imposing the condition for projecting the number of particles) is plotted with a thin line. The dissipated energy obtained by replacing the ground state of the parent nucleus within the ground states of the two nascent fragments is displayed with a dashed line. (b) The number of pairs N_{p_1} and N_{p_2} located on the levels that belong to the first and second well are plotted with thick lines in the framework of the TDPE. The number of pairs within the TDPEC are plotted with thin lines. N_{p_2} corresponds to the heavy fragment and it is always larger than N_{p_1}.

also for relation (16), k_1 and k_2 are levels in the active pairing space attributed to fragment 1 and to fragment 2, respectively. The total number of pairs is conserved: $N_1 + N_2 = N = 30$. After imposing condition (20), the numbers of pairs located on the two-level schemes of the two fragments reach the correct values, that is, $N_1 = 15$ and $N_2 = 15$, that define the partition analyzed.

It was remarked in Ref. [31] that the maxima of the dissipated energy arise because the character of the ground-state solution is changing so rapidly that the system cannot adjust itself. Thus, the system appears excited, not because of any large changes in the occupation amplitudes but because of the changes in the ground state to which the dynamic state is studied. In this respect, in Fig. 7, we also analyzed the behavior of the system by replacing the ground state. Instead of the ground state of the parent E_0, we used $E_{01} + E_{02}$, that is, the sum between the BCS lower energy states calculated within the level schemes attributed to the two nascent fragments. Within this modification, the true dissipation energy of the fragments is obtained with relation (15). The result is plotted with a dashed line. At scission we obtain approximately 8 MeV as the neutron contribution in the dissipated energy. The proton contribution is calculated in the same way.

Having the dynamical occupation probabilities together with the BCS solutions and the level schemes of the nascent nuclei, it is possible to evaluate the excitation energy separately for an individual fragment. As mentioned previously, a strong dependence exists between the collective velocity and the total dissipation released in fission. Therefore, it is possible to emphasize the correlation between the modality in which the excitation is shared between fragments and the total excitation energy by appealing to the internuclear velocity. In Fig. 8, the dissipation energies obtained for each of the two fragments are displayed separately as a function of the collective velocity. The total excitation energy is the sum between the contributions of the two fission products. It is found that the dissipated energy for the heavy fragment is much lower than that for the light one. This result is consistent with the experimental finding addressing the neutron multiplicities. The number of evaporated neutrons is directly proportional to the E^* of the fragment. In the 0.8-MeV neutron-induced fission of ^{237}Np [8], the number of evaporated neutrons from the heavy fragment of mass 132 is about half of that emitted from the light partner. In our calculations, the excitation energy accumulated in the heavy fragment is also about half of the excitation obtained in the light one. It is also revealed in Fig. 8 that in the low energy regime the increase in excitation energy of the heavy fragment is smaller than in the light one, for a modification of the total excitation energy of the parent nucleus. However, the experimental findings [8] show that the excitation energy of the compound nucleus goes almost completely into excitation energy of the heavy fragments. We can speculate that a large part of this energy is transferred in deformations of the heavy nucleus, not taken into account here. A similar behavior is assessed from statistical considerations in Ref. [3], and detailed in Ref. [51], for energy partitions involving nuclei close to magic numbers.

In the present work, TDPEC are derived involving the variational principle in a way similar to that of Ref. [32].

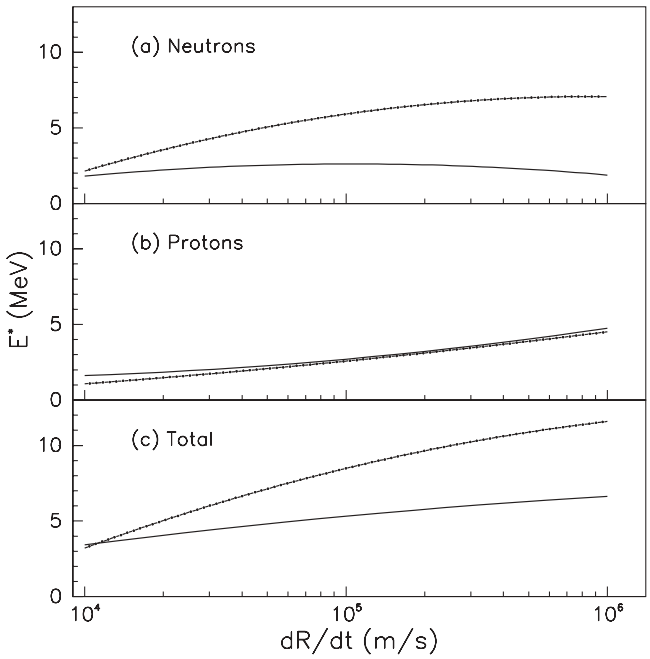

FIG. 8. Excitation energies for ^{102}Zr (dashed line) and ^{132}Te (solid line) as a function of the internuclear velocity dR/dt. The excitations after scission are displayed for the (a) neutron and (b) proton contributions. (c) The total dissipation energies accumulated in each fragment are presented with the same line types.

Alternatively, in Ref. [31], system (14) is obtained from the Heisenberg form of the equations of motion. In this treatment, a full solution of the dynamics describing the time evolution emerges that reflects more accurately the response of the nuclear system to the changing single-particle potential. It was shown in Ref. [18] that the two derivations give the same results when the antisymmetric time-derivative matrix of the wave function is explicitly taken into account. The collective kinetic energy associated to the coherent movement of the nucleons is revealed in terms of a nonadiabatic cranking inertia. According to a classification made in Ref. [2], the model used in the present work belongs to a family in which the dissipation can be identified with the excitation obtained within coupled-channel equations, as in Refs. [31,52,53]. Another important family of models solves equations of motion and extracts the excitation energy by following the trajectory backward with reversed velocity as in Ref. [54].

This model is based on the same fundamental grounds as those found in Refs. [47,55]. The main differences are given by the time-dependent equations used and by the fact that the dissipation is not evaluated for each fragment separately. They used the time-dependent Schrödinger equations and introduced quasiparticle excitations through the cranking approximation.

VII. CONCLUSIONS

Dynamical estimations of the excitation energies in cold fission are evaluated within time-dependent pairing equations. Using conditions that fix the number of particles in each fragment, it was possible to obtain for the first time the excitation energy of each nucleus issued in the process. A recent hypothesis [3] that claims the excitation energy is not equilibrated between fragments was confirmed in the cold fission regime. If the heavy fragment is close to magic number, its excitation energy is smaller than that of the light one. It was found that the dissipation energy in fission fragments is intimately related to the distribution of pairing occupation probabilities of the levels at scission. These probabilities can be obtained by solving an appropriate set of equations of motion.

ACKNOWLEDGMENTS

This work was performed in the frame of Projects IDEI No. 512 and MODUL III No. EU65 of the Romanian Ministry of Education and Research.

[1] I. S. Grant, Rep. Prog. Phys. **39**, 955 (1976).
[2] R. W. Hasse, Rep. Prog. Phys. **41**, 1027 (1978).
[3] K.-H. Schmidt and B. Jurado, Phys. Rev. Lett. **104**, 212501 (2010).
[4] H. A. Bethe, Phys. Rev. **50**, 332 (1936).
[5] H. R. Bowman, S. G. Thomson, J. C. D. Milton, and W. J. Swiatecki, Phys. Rev. **126**, 2120 (1962).
[6] V. F. Apalin, Yu. N. Gritsyuk, I. E. Kutinov, V. I. Lebedev, and L. A. Mikaelian, Nucl. Phys. **71**, 553 (1965).
[7] S. C. Burnett, R. L. Ferguson, F. Plasil, and H. W. Schmitt, Phys. Rev. C **8**, 2034 (1971).
[8] A. A. Naqvi, F. Käppeler, F. Dickmann, and R. Müller, Phys. Rev. C **34**, 218 (1986).
[9] M. Mirea, Phys. Rev. C **78**, 044618 (2008).
[10] M. Brack, J. Damgaard, A. S. Jensen, H. C. Pauli, V. M. Strutinsky, and C. Y. Wong, Rev. Mod. Phys. **44**, 320 (1972).
[11] U. Brosa, S. Grossman, and A. Muller, Phys. Rep. **197**, 167 (1990).
[12] J. R. Nix, Annu. Rev. Nucl. Sci. **22**, 65 (1972).
[13] M. Mirea, R. C. Bobulescu, and M. Petre, Rom. Rep. Phys. **61**, 646 (2009).
[14] M. Petre, R. C. Bobulescu, C. Petre, and M. Mirea, Rom. J. Phys. **55**, 741 (2010).
[15] K. T. R. Davies and J. R. Nix, Phys. Rev. C **14**, 1977 (1976).
[16] M. Mirea, O. Bajeat, F. Clapier, F. Ibrahim, A. C. Mueller, N. Pauwels, and J. Proust, Eur. Phys. J. A **11**, 59 (2001).
[17] P. Moller and J. R. Nix, At. Data Nucl. Data Tables **26**, 165 (1981).
[18] M. Mirea and R. C. Bobulescu, J. Phys. G **37**, 055106 (2010).
[19] V. V. Samarin, Phys. At. Nucl. **73**, 1416 (2010).
[20] A. Diaz-Torres and W. Scheid, Nucl. Phys. A **757**, 373 (2005).
[21] S. Cwiok, J. Dudek, W. Nazarewicz, J. Skalski, and T. Werner, Comput. Phys. Commun. **46**, 379 (1987).
[22] J. Maruhn and W. Greiner, Z. Phys. **251**, 431 (1972).
[23] M. Mirea, Phys. Rev. C **54**, 302 (1996).
[24] M. Mirea, Nucl. Phys. A **780**, 13 (2006).

[25] M. Mirea, D. S. Delion, and A. Sandulescu, Phys. Rev. C **81**, 044317 (2010).
[26] M. Mirea, D. S. Delion, and A. Sandulescu, Europhys. Lett. **85**, 12001 (2009).
[27] M. Mirea, Phys. Rev. C **57**, 2484 (1998).
[28] M. Mirea, Eur. Phys. J. A **4**, 335 (1999).
[29] M. Mirea, Phys. Rev. C **63**, 034603 (2001).
[30] M. Mirea, L. Tassan-Got, C. Stephan, and C. O. Bacri, Nucl. Phys. A **735**, 21 (2004).
[31] S. E. Koonin and J. R. Nix, Phys. Rev. C **13**, 209 (1976).
[32] J. Blocki and H. Flocard, Nucl. Phys. A **273**, 45 (1976).
[33] M. Mirea, Mod. Phys. Lett. A **18**, 1809 (2003).
[34] M. Mirea, Phys. Lett. B **680**, 316 (2009).
[35] D. S. Delion, M. Baldo, and U. Lombardo, Nucl. Phys. A **593**, 151 (1995).
[36] R. C. Kennedy, Phys. Rev. **144**, 804 (1966).
[37] J. Dobaczewski, W. Nazarewicz, T. R. Werner, J. F. Berger, C. R. Chinn, and J. Decharge, Phys. Rev. C **53**, 2809 (1996).
[38] P. Moller, A. J. Sierk, T. Ichikawa, A. Iwamoto, R. Bengtsson, H. Uhrenholt, and S. Aberg, Phys. Rev. C **79**, 064304 (2009).
[39] R. Smolanczuk, J. Skalski, and A. Sobiczewski, Phys. Rev. C **52**, 1871 (1995).
[40] Z. Patyk, J. Skalski, A. Sobiczewski, and C. Cwiok, Nucl. Phys. A **502**, 591c (1989).
[41] A. Dobrowolski, K. Pomorski, and J. Bartel, Phys. Rev. C **75**, 024613 (2007).
[42] D. N. Poenaru, M. Mirea, W. Greiner, I. Cata, and D. Mazilu, Mod. Phys. Lett. A **5**, 2101 (1990).
[43] M. Mirea, L. Tassan-Got, C. Stephan, C. O. Bacri, P. Stoica, and R. C. Bobulescu, J. Phys. G **31**, 1165 (2005).
[44] M. Mirea, L. Tassan-Got, C. Stephan, C. O. Bacri, and R. C. Bobulescu, Europhys. Lett. **73**, 705 (2006).
[45] M. Mirea, L. Tassan-Got, C. Stephan, C. O. Bacri, and R. C. Bobulescu, Phys. Rev. C **76**, 064608 (2007).
[46] M. Mirea and L. Tassan-Got, Cent. Eur. J. Phys. **9**, 116 (2011).
[47] T. Ledergerber, Z. Paltiel, Z. Fraenkel, and H. C. Pauli, Nucl. Phys. A **275**, 280 (1977).
[48] A. C. Wahl, At. Data Nucl. Data Tables **39**, 1 (1988).
[49] S. Pilat, K. Pomorsky, and A. Staszczak, Z. Phys. A **332**, 259 (1989).
[50] W. J. Swiatecki and S. Bjornholm, Phys. Rep. **4**, 325 (1972).
[51] K.-H. Schmidt and B. Jurado, Phys. Rev. C **83**, 014607 (2011).
[52] S. E. Koonin, R. L. Hatch, and J. Randrup, Nucl. Phys. A **283**, 87 (1977).
[53] D. Glas and U. Mosel, Phys. Nucl. Phys. A **264**, 268 (1976).
[54] G. Schutte and L. Wilets, Nucl. Phys. A **252**, 21 (1975).
[55] T. Ledergerber, Z. Patiel, H. C. Pauli, G. Schutte, Y. Yariv, and Z. Fraenkel, Phys. Lett. B **56**, 417 (1975).